Materials Advances

ROYAL SOCIETY OF CHEMISTRY

PAPER

View Article Online
View Journal | View Issue

Cite this: *Mater. Adv.*, 2024, 5, 1930

A blue phase liquid crystal film based on an interpenetrating network and its sensitive humidity response performance†

Wentuo Hu, Wanli He,* Kainan Wang, Changli Zhang, Zhou Yang, Yuzhan Li, Hui Cao and Dong Wang

Received 30th October 2023,
Accepted 5th January 2024

DOI: 10.1039/d3ma00931a

rsc.li/materials-advances

A humidity-responsive blue phase liquid crystal polymer film (alkalized-acrylic-BP) based on an interpenetrating polymer system has been fabricated. The nanostructure of the blue phase liquid crystal polymer was manipulated *via* interpenetrating networks (IPNs) by sequential synthesis into a humidity-sensitive acrylic acid, which exhibited sensitive response behavior to changes in humidity. The moisture response ability of the film was investigated by examining various influencing factors, while characterizing the color and shape changes induced by humidity. A comparison was made between the micromorphology differences of blue phase and cholesteric phase samples, as well as the reflectance changes influenced by humidity. The film exhibits not only humidity-induced color changes, but also demonstrates excellent deformation response performance, thereby showcasing its potential for advanced applications such as sensors, displays, and anti-counterfeiting.

1. Introduction

Due to its unique structural composition, liquid crystal materials possess the ability to react to a diverse range of external stimuli (such as temperature,[1–4] electricity,[5,6] light[7,8] and organic gas[9–12]). Therefore, they are frequently utilized in the creation of stimulus-response materials. Currently, cholesteric liquid crystals (CLCs) are the most prevalent type of liquid crystal materials that exhibit humidity-responsive behavior. Researchers utilized the high sensitivity of hydrogen bond units to environmental chemical stimuli and employed them as molecular triggers in cholesteric liquid crystals[13] to fabricate heat-exchanging reflective color films and optical sensors[14,15] to respond to water and pH.[16–19] Yu *et al.* used water to achieve a series of large complex non-contact motions, as well as dual-mode actuation of UV light, through azobenzene containing cross-linked liquid crystal polymer films without hydrophilic groups.[19] Stumpel *et al.* used a cholesteric liquid crystal network interwoven with a polyacrylic acid network to obtain patterned coating colors for static interpenetrating polymer network regions with a humidity and pH response.[17]

Compared to conventional cholesteric liquid crystals with one-dimensional nanostructures, blue phase liquid crystals (BPLCs) possess unique three-dimensional nanostructures that endow them with several intriguing and advantageous properties, including rapid response times, narrow photonic band gaps, and the ability to avoid complex molecular arrangements.[20–24] Many researchers have explored the BPLC stimulus response.[13,25–30] Hu *et al.* designed a large number of hydrogen bond units and a high proportion of polymerizable monomers to construct a self-assembled three-dimensional nanostructure of BPLCSs and generate independent BPLCSs with humidity-responsive behavior.[31] Yang *et al.* designed a moisture-driven chromogenic photonic polymer coating of a hydrogen-bonded 3D blue-phase liquid crystal network which could achieve a moisture-driven reversible color change in the visible spectrum upon breaking the hydrogen bond and subsequent conversion to a hygrophilic polymer coating.[32] However, due to the special structure of BPLCSs, their chemical composition and composition ratio are greatly limited, and usually exist in a narrow temperature range.[17,28,33–35] For example, polymer networks,[36] nanoparticles[23] or curved core molecules[37] may be used to stabilize their own morphology, which greatly affects the fabrication of blue-phase liquid-crystal stimulus response devices. At present, the response of blue-phase liquid crystal materials to humidity stimulation is relatively simple, which limits the application of blue-phase liquid crystal polymers. Therefore, it is necessary to develop a variety of humidity response forms, which can help improve the humidity response performance of the blue phase.

The utilization of interpenetrating polymer networks (IPNs) is prevalent in amalgamating the desired properties and

Department of Materials Science and Engineering, University of Science and Technology Beijing, Beijing, 100083, China. E-mail: hewanli@mater.ustb.edu.cn

† Electronic supplementary information (ESI) available. See DOI: https://doi.org/10.1039/d3ma00931a

augmenting the functionality of constituent polymers within a given structure.[38] In recent years, IPNs have been greatly developed in various fields, such as biology,[39,40] electrochemistry,[41,42] mechanics,[43] medical materials,[44] sensors,[45] *etc.* IPNs based on liquid crystal polymer networks have been widely used in optical sensing applications for the detection of light,[46,47] temperature,[48] water,[16,17] volatile organic compounds,[49] ions,[50] *etc.* The IPN structure can also be used to construct humidity-responsive polymer systems, but the combination of blue-phase liquid crystal polymers with IPNs has not been reported. Therefore, a humidity-responsive blue phase liquid crystal polymer film (alkalized-acrylic-BP) based on IPNs was designed in this paper. The hydrogen bond units retained by the interlaced polyacrylic acid network in the film were used as the trigger factor for the response behavior, which was very sensitive to the external humidity change. The blue phase structure in the film retained its liquid crystal state while successfully integrating the blue phase liquid crystal polymer and polyacrylic acid. Finally, the functional film exhibits deformability and chromaticity changes in response to humidity signals, making it suitable for non-contact electronic devices. This study sheds new light on the integration of blue-phase liquid crystal materials with hydrogels and expands the potential applications of blue-phase liquid crystal polymers in electronic devices and sensors.

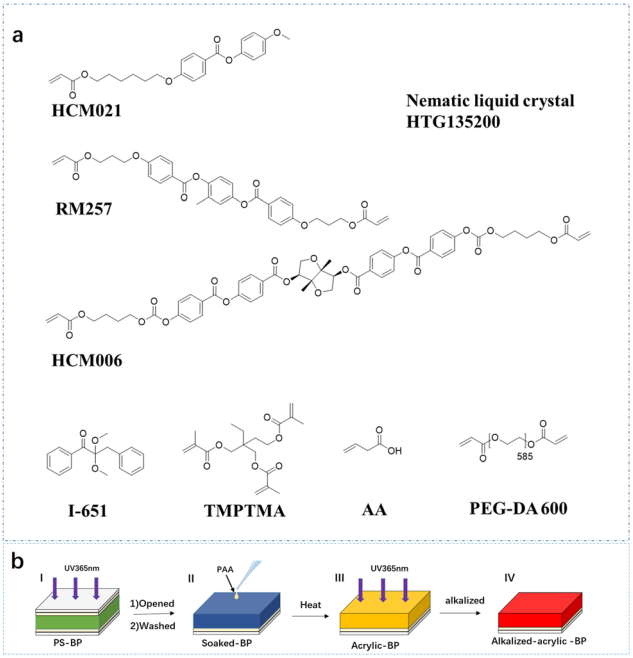

Fig. 1 (a) Molecular structure of the compounds used in this paper. (b) Flowchart of the preparation of a humidity-responsive blue phase liquid crystal film at each stage.

2. Results and discussion

2.1. Construction of blue phase liquid crystal films with a humidity response in the IPN system.

The humidity response process of alkalized-acrylic-BP is different from the previously reported humidity response process of blue phase liquid crystals.[31,32] The expansion of the IPN network is driven by the sensitivity of the poly acrylic acid network to external humidity, utilizing the mechanism of acrylic water absorption and expansion. Consequently, this leads to an increase in lattice spacing of the blue phase liquid crystal polymer due to the expansion of both networks. The texture color of the blue phase liquid crystal was consequently altered, leading to a redshift in the reflection peak. During the dehydration process, water was lost from the poly acrylic acid network, leading to a shrinkage of the IPN film and a consequent reduction in lattice spacing. Consequently, a blue shift in reflection was observed. At the same time, the blue phase liquid crystal network itself also has a good shape memory ability,[51] which also makes this process has good repeatability.

In order to prepare an IPN type humidity-responsive blue phase liquid crystal film, an acrylic ester monomer, a crosslinking agent, a chiral dopant, a photoinitiator and a nematic liquid crystal **HTG135200** with a single functional group are used in this study. The specific molecular structure is shown in Fig. 1. Specifically, **HTG135200** acts as the liquid crystal body. **RM257** and **HCM021** are used to form chemically cross-linked BP networks. **HCM006** also acts as a crosslinker and as a chiral additive, inducing chiral nematic phases through its high helical torsional ability. **TMPTMA** was added to stabilize the BP structure, and **I-651** was used to initiate the photopolymerization process and freeze the phase. The preparation procedure of the humidity-responsive blue phase liquid crystal polymer film is illustrated in Fig. 1b (**HTG135200** = 30.0 wt%, **RM257** = 15.0 wt%, **HCM006** = 6.0 wt%, **TMPTMA** = 1.5 wt%, and **I-651** = 1.0 wt%).

In this formulation, the liquid crystal mixture is thoroughly mixed and filled into a liquid crystal cell by capillary force at 60.0 °C. The sample is then heated to the isotropic phase and carefully cooled at a rate of 0.05 °C min^{-1} to obtain the BP phase. At a temperature 1.0 °C higher than the phase transition temperature from BP to Ch, the PS-BP film is obtained by irradiating the sample with 5.0 mW cm^{-2} ultraviolet light (365 nm) for 600 seconds. The thermal stability and temperature range of the samples before and after polymerization were measured using a polarizing microscope (POM). The cooling process of this component sample reveals a BP texture ranging from 58.0 °C to 53.5 °C, as illustrated in Fig. S1 in the ESI.† The phase transition temperatures for samples of other components involved in subsequent experiments were determined using the same method, as presented in Table 1.

The second step involves opening the liquid crystal cell, immersing the PS-BP film in THF for a duration of 6 hours, rinsing off the unreacted liquid crystal **HTG135200**, and subsequently drying it to obtain soaked-BP. As can be observed from Fig. 2a, due to the contraction of the crystal lattice[27] after washing off the liquid crystal, the reflection spectra of the film moved from the original position at about 528 nm to about 425 nm compared to PS-BP and soaked-BP. The SEM image of the PT-BP surface morphology also shows that there are some holes on the surface of the film. The removal of **HTG135200** was confirmed through infrared (FT-IR) spectroscopy analysis, as depicted in Fig. 3. Specifically, the characteristic signal peak

Table 1 Table of experimental component contents

Sample	HTG135200 (wt%)	RM257 (wt%)	HCM006 (wt%)	Wavelength shift value ($\Delta\lambda$)	BP range[a] (°C)
1	20.0	10.0	6.0	63.81	50.4–44.5
2	20.0	15.0	6.5	38.33	50.9–44.5
3	20.0	18.0	7.0	50.40	51.2–45.1
4	30.0	15.0	6.0	57.95	55.7–51.5
5	30.0	18.0	6.5	41.61	55.8–52.4
6	30.0	10.0	7.0	44.55	54.7–51.8
7	40.0	18.0	6.0	70.88	58.0–53.5
8	40.0	10.0	6.5	40.56	57.6–52.7
9	40.0	15.0	7.0	54.69	59.7–54.2

[a] All of the phase transition temperatures were tested on cooling.

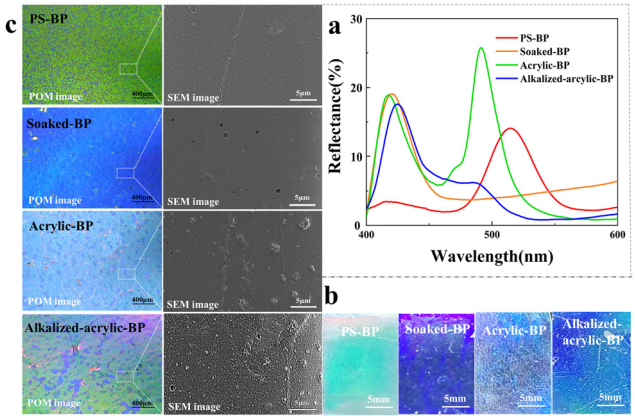

Fig. 2 (a) Reflection spectra of samples at different stages. (b) Picture of the real products. (c) Comparison of the POM diagram and the SEM diagram of the surface morphology of each sample.

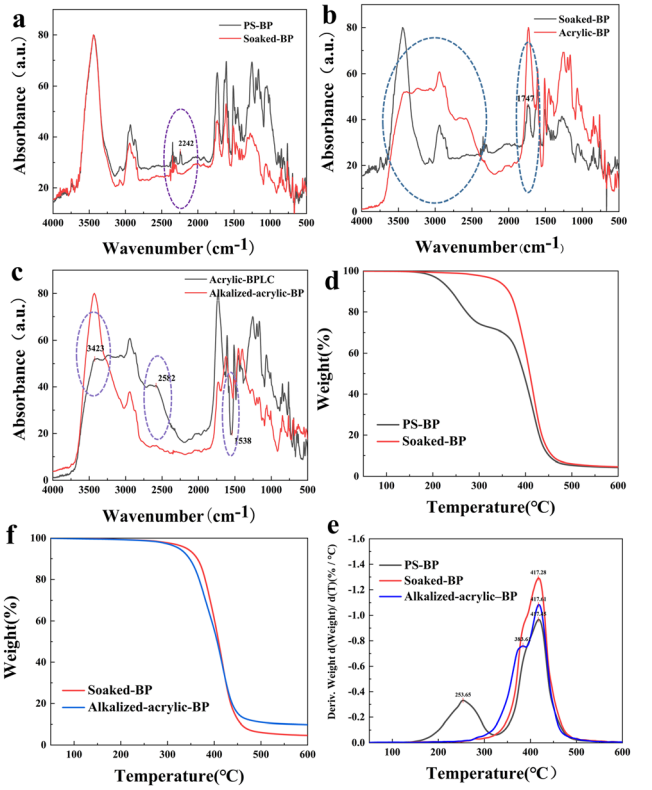

Fig. 3 (a)–(c) Infrared spectra of samples at various stages. (d) and (e) Thermogravimetric analysis of samples at various stages.

at 2242 cm^{-1} corresponding to the cyanide bond vanished (Fig. 3a). By comparing the thermogravimetric curve of PS-BP with that of soaked-BP, it was observed that the thermogravimetric curve of PS-BP exhibited a gradual decline starting at 253.65 °C. Subsequently, a plateau emerged in the curve, indicating a loss in the mass fraction of approximately 30%. Remarkably, this value precisely corresponds to the quantity of **HTG135200** present, thereby demonstrating the complete removal of free small molecule liquid crystals through THF washing and leaving behind only the polymer network.

In the third step, the entire soaked BP film is swelled with PAA (**AA : PEG-DA 600 : I-651** = 98 : 1 : 1 wt%) and irradiated with 2.5 mW cm^{-2} ultraviolet light (365 nm) at 60 °C for 600 seconds to obtain Acrylic BP. Compared with soaked-BP, acrylic-BP presents a new peak at 492 nm. The texture of the entire film shown in the POM image in Fig. 2c reveals two distinct regions, attributed to the multi-domain nature of the blue phase lattice. This phenomenon can be attributed to partial filling of the crystal lattice by PAA, while other areas remain unfilled, resulting in the appearance of two peaks. The lattice components are prominently observable in the POM diagram of PS-BP and soaked-BP, wherein the blue phase network undergoes expansion while the pitch increases subsequently to acrylic penetration. Infrared spectra show signals from 1800 to 1650 cm^{-1}, with strong peaks indicating the presence of carboxylic acids (Fig. 3b). Through the SEM map of the surface topography of soaked-BP shown in Fig. 2, some substance embedding can be seen in some areas of the sample surface before and after soaking acrylic, which is presumed to be PAA after IPN treatment. The combined data show that IPN of the polyacrylic acid and polymer BPLC network has been formed.

Finally, the BP film is immersed in a 0.1 mol L^{-1} KOH solution to eliminate excess polyacrylic acid. Subsequently, the film is detached from the glass substrate, leading to activation of acrylic acid into acrylates and thereby enhancing the overall humidity response of the film. Consequently, the alkalized-acrylic-BP with excellent humidity sensitivity was obtained. Compared to the reflection spectrum shown in Fig. 2a, the reflection peak of the second alkalized acrylic-BP at 525 nm is attenuated and exhibits a blue shift of 5–10 nm. This can be attributed to the removal of excess acrylic acid, as confirmed by SEM analysis revealing changes in the surface morphology of alkalized acrylic-BP. The film's surface roughness is significantly increased, leading to a substantial decrease in its reflectivity. It can also be clearly seen from the POM diagram of alkalized acrylic-BP in Fig. 2 that the whole blue texture has two parts, one of which is blue texture. The blue texture's main reflection peak is at about 425 nm, which we guess is due to the pure polymerizable monomer and it cannot be swelled with PAA. In the other part, due to the gap of **HTG135200** after washing, it presents a green texture after IPN treatment, and its reflection peak will move with the change of external conditions. This feature is significantly

different from that of the CLC humidity responsive films reported in previous literature.[17] In the infrared spectrum shown in Fig. 3c, there are wide and scattered stretching vibration absorption peaks of –OH in the range of 2500–3300 cm^{-1}, which increase in intensity and decrease in width after alkalization. Because the LC film containing acrylic acid contains a lot of carboxylic acid, the signal saturation occurs in the range of 1800–1650 cm^{-1}. After alkalization, the infrared signal is weakened, and the signal appears at around 1538–1573 cm^{-1}, indicating the formation of carboxylate ions. A comparison of the thermogravimetric curves of alkalized acrylic-BP and soaked-BP is shown in Fig. 3f, and the trend of the thermogravimetric curves of both is similar. However, the alkalized acrylic-BP experiences a decrease in temperature to 250 °C due to the influence of PAA. Conversely, the TG curves of soaked-BP exhibit a decline at approximately 320 °C (Fig. 3e).

2.2. Influencing factors of humidity responsive blue phase liquid crystal films in the IPN system

The factors influencing the humidity response of alkalized-acrylic-BP films were studied by grouping the contents of different components. The reflectance of the sample after adding water was measured (Table 1 and Fig. 4). Both the change of the reflectance of the sample ($\Delta\lambda$) and the average $\Delta\lambda(K_{avg}\Delta\lambda)$ were analysed (the specific calculation and analysis process is shown in S2, ESI†). By calculating the average $K_{avg}\Delta\lambda$ values of the levels under each factor, it was found that the reflectance of the water-responsive film increases with the increase of the **RM257** content. This suggests a potential positive correlation between the **RM257** content and the average change in film reflectance ($K_{avg}\Delta\lambda$). Subsequently, this conclusion has been independently verified using experimental samples 8, 10, and 11 (Table 2 and Fig. 6), demonstrating an increase in the reflection peak shift with higher **RM257** content. The presence of **RM257**, a bifunctional crosslinking agent, exerted a significant influence

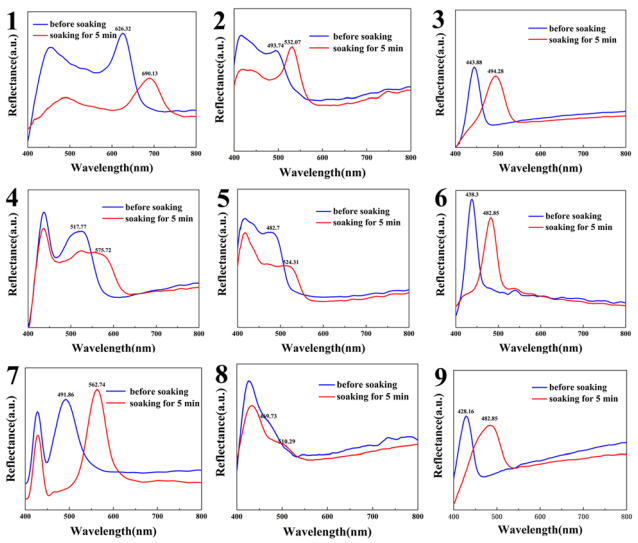

Fig. 4 Reflection spectra of the sample (1–9) under the influence of humidity.

Table 2 Table of experimental components in the verification group

Sample	**HTG135200** (wt%)	**RM257** (wt%)	**HCM006** (wt%)	Wavelength shift value ($\Delta\lambda$)	BP range[a] (°C)
8	40.0	10.0	6.5	40.56	57.6–52.7
10	40.0	7.0	6.5	36.16	57.3–52.2
11	40.0	5.0	6.5	21.42	56.9–51.8

[a] All of the phase transition temperatures were tested on cooling.

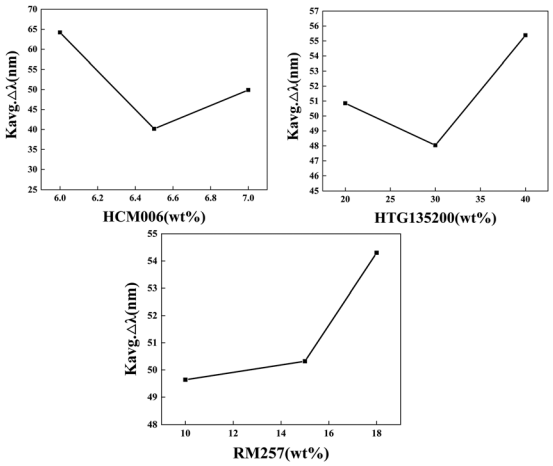

Fig. 5 The variation trend of $K_{avg}\Delta\lambda$ with **HTG135200**, **RM257** and **HCM006** contents.

on the overall film's quality in terms of its formation. The impact of **HCM006** and **HTG135200** on the $K_{avg}\Delta\lambda$ value exhibited a complex pattern, characterized by an initial decrease followed by a subsequent increase (Fig. 5). Through analysis of the experimental data, it has been determined that various components of alkalized acrylic-BP exhibit humidity response, thus demonstrating the feasibility of this approach. The alkalized acrylic-BP exhibited two distinct peaks, with the first peak of samples 2, 5, and 8 closely appearing at a wavelength of approximately 400 nm. However, samples 3, 6, and 9 only displayed a single peak. It was speculated that the presence of a high mass fraction of the chiral molecule **HCM006** may account for the observed only single peak for Samples 3, 6, and 9. The original peak after washing occurs at wavelengths beyond the measurement range of our instrument, specifically exceeding to 400 nm. Through the screening of the experimental data, within the range of experimental data in this paper, we obtained an optimal formula (sample 7 **HTG135200** = 40.0 wt%, **RM257** = 18.0 wt%, and **HCM006** = 6.0 wt%), and subsequent experiments were carried out according to this formula.

2.3. Performance of blue phase liquid crystal films in the IPN system

Based on the experimental conclusions discussed in section 2.2, the best experimental formula was identified for the above experimental groups for subsequent patternization experiments (sample 7 **HTG135200** = 40.0 wt%, **RM257** = 18.0 wt%,

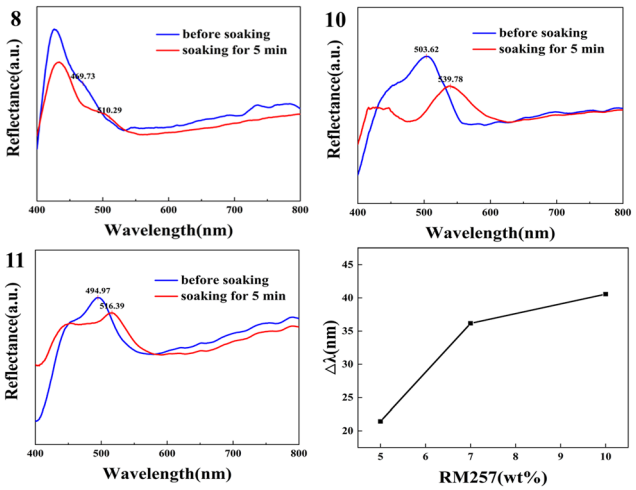

Fig. 6 Effect of changing the **RM257** content on $\Delta\lambda$ alkalized acrylic-BP reflection spectra (samples 8, 10, and 11).

HCM006 = 6.0 wt%, **TMPTMA** = 1.5 wt%, **I-651** = 1.0 wt%). The changes in the dry film and after exposure to humidity are investigated, as depicted in Fig. 7a.

Obvious color changes can also be observed from the physical pictures and POM images. At the same time, the film also expanded and the surface area increased. Under the stimulation of humidity, the POM images of the film also indicated the redshift of the blue-phase texture. The reflection spectrum in Fig. 7c reveals that the blue phase network within the polyacrylic acid expands upon exposure to humidity, resulting in a redshift of the reflection spectrum from 491 nm to approximately 542 nm and the emergence of surface folding on the film. The results demonstrated the excellent responsiveness of the alkalized-acrylic-BP film to external humidity stimulation, as evidenced by the observed increase in the pitch, redshift in the

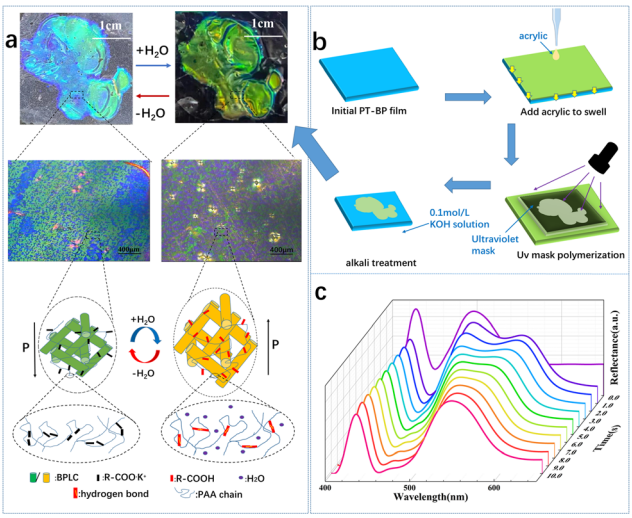

Fig. 7 (a) The patterned physical diagram, POM image, and mechanism diagram of the alkalized-acrylic-BP film and after humidity response. (b) Humidity response pattern making diagram. (c) Temporal changes in the reflection peak following film soaking.

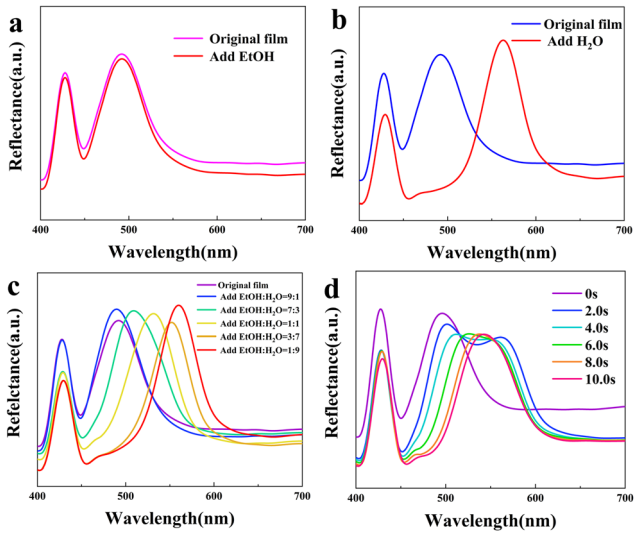

Fig. 8 (a) Reflection spectrum of alkalized-acrylic-BP dripped with EtOH. (b) Reflection spectrum of alkalized-acrylic-BP dripped with H_2O. (c). Alkalized acrylic – BP dripped with mixed solutions of EtOH and H_2O. (d) Reflection spectrum of alkalized-acrylic-BP dripped with H_2O within 10 s.

reflection spectrum, and alterations in the surface area. Simultaneously, the temporal evolution of the alkalized-acrylic-BP reflection spectra under varying external humidity conditions revealed a duration of approximately 10 seconds for the entire process.

In order to further investigate the mechanism underlying the humidity response, a series of mixed solutions with varying mass fractions of H_2O and EtOH were dripped onto alkalized acrylic-BP, followed by an investigation into the impact of ethanol–water mixtures on the reflective properties of alkalized acrylic-BP. The initial reflection was around 491 nm. When 100%EtOH was dripped onto the film as shown in Fig. 8a, no discernible shift of the reflection peak was observed, indicating the lack of the response of the film towards EtOH. Therefore, EtOH can serve as a contrasting solution for alkalized acrylic-BP when dripped in combination with water. Next, mixed solutions of EtOH and H_2O with different mass fractions were dripped onto dry alkalized acrylic-BP, respectively. The reflection peak of the entire film gradually undergone a redshift to approximately 542 nm as the H_2O content increased. By observing the change of the reflection spectrum of the whole alkalized acrylic-BP added with H_2O within 10 s in Fig. 8d, it can be concluded that the reflection peak changed in the process. The reflection peak did not move directly. It first appeared in the corresponding position after H_2O was introduced, and then the original reflection peak gradually disappeared. Finally, the entire reflection peak shifted.

2.4. Deformation of films under the influence of humidity

It can be observed from the physical diagram in section 2.3 that the film also has a deformation phenomenon while undergoing color changes. The optimal ratio of materials was chosen from Table 1, sample 7. Upon exposure to humidity (Fig. 9a), the alkalized-acrylic-BP film exhibited rapid curling within 30

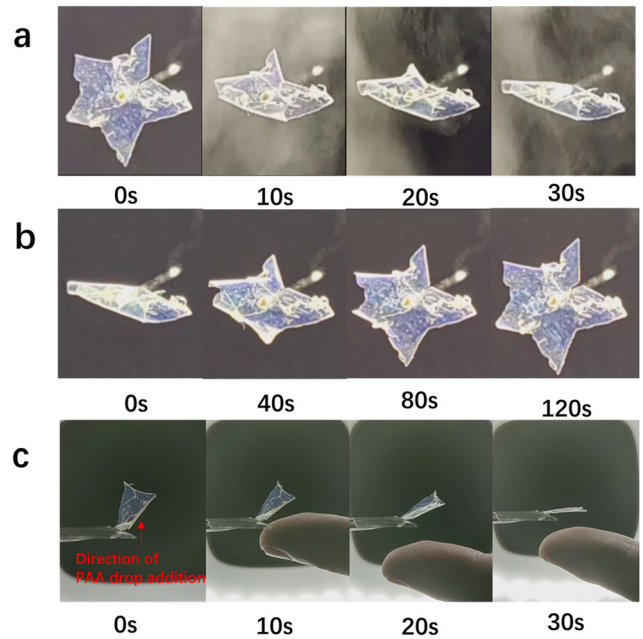

Fig. 9 (a) Deformation process of alkalized-acrylic-BP under external humidification conditions. (b) Alkalized acrylic-BP recovery process in a natural environment after humidity removal. (c) The film consistently exhibits unidirectional bending when observed closely with a finger.

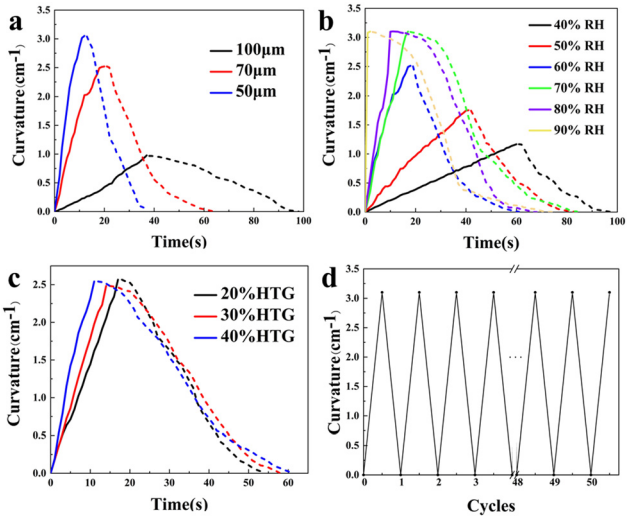

Fig. 10 (a) Curvature change diagram of alkalized-acrylic-BP films with different thicknesses under 70%RH difference (solid line) and the subsequent membrane recovery process (dotted line). (b) The difference diagram of the 70 μm thickness film exposed to different humidities (solid line) and the subsequent membrane recovery process (dotted line). (c) Curvature change diagram of 70 μm films with different **HTG135200** contents at 70%RH (solid line) and the subsequent membrane recovery process (dotted line). (d) Diagram showing reversible deformation of the film at cyclic exposure to an 80% RH difference. Humidity-induced experiment is repeated for up to 50 cycles without noticeable fatigue.

seconds as external moisture levels increased. Upon removal of the applied humidity (Fig. 9b and mov. s1, ESI†), the film gradually reverted to its original state within 120 seconds as moisture evaporated, with complete reversibility of surface bending. Moreover, when the finger approached the film from either direction, it exhibited a spontaneous curvature towards the dropwise acrylic side (Fig. 9c and mov. s2, ESI†).

Because the direction of acrylic water absorption expansion was not regular, the bending direction of the entire film was likely to be affected by acrylic acid during the preparation process, and the film was completely swollen by acrylic acid, after the removal of excess acrylic acid, the amount of acrylic acid on the back of the film was more, affecting the direction of the film bending. When in contact with H_2O, the film always bends towards the side of the drop added acrylic acid, which may impact its bending direction. The results clearly indicated that even a slight increase in local humidity near the film can induce rapid bending, and the film demonstrates high sensitivity to exposed human skin. Additionally, the film was affixed to a metal wire and grounded for connectivity. The influence of static electricity on the film was eliminated by grounding the metal wire with a finger (Fig. S3, ESI†), indicating that the humidity was responsible for inducing the bending of the film rather than static electricity. Furthermore, the placement of a film on the surface of a rubber glove did not result in any bending, thus indicating that the temperature gradient is not responsible for the observed bending behavior.

By making a self-made humidity chamber with small holes (Fig. S4, ESI†), the curvature k (cm^{-1}) was determined following the methodology outlined in Fig. S3, ESI.†[19] The quantitative analysis of the effects of relative humidity differences, the film thickness, **HTG135200**, and film type on the bending curvature and speed was conducted to elucidate the control mechanism of actuation. Fig. 10b illustrates the bending behavior of alkalized acrylic-BP films with varying thicknesses under a relative humidity (RH) difference of 70%. Films with varying thicknesses exhibit sensitivity to external humidity. For instance, a film measuring 70 μm in thickness demonstrated a steady-state curvature of 2.5 cm^{-1}. The experimental results demonstrated that the bending speed and curvature of the film largely depend on the film thickness. Fig. 10c illustrates the variations in the film curvature induced by different levels of humidity, ranging from approximately 40% to roughly 90% relative humidity, and the film thickness measured 70 μm. As the difference in relative humidity increased from 40% to 90%, there was a gradual increase in the steady-state bending curvature of the film. At an external relative humidity of 70%, the film exhibited the maximum curvature. We hypothesize that acrylic acid in the film replaces the original **HTG135200** within the blue phase network, thereby influencing the humidity response of the film depending on its **HTG135200** content. The humidity response curvature of the film at 70%RH is illustrated in Fig. 10c, with varying **HTG135200** contents (selected as samples 2, 4, and 9 in Table 1). The experiment revealed that the film's humidity response rate was most rapid at 40% **HTG135200** content, which aligns with our prior conjecture. The selected thickness was 70 μm, and the sample group was denoted sample 7. Under an environmental condition of 80%RH, the film's humidity response process was

repeated over 50 times without exhibiting noticeable fatigue (Fig. 10d). The experimental results demonstrate the consistent and dependable humidity response of the alkalized acrylic-BP film, thereby highlighting its repeatability and reliability.

2.5. Comparison of the humidity response between the blue phase liquid crystal polymer and the cholesteric phase liquid crystal polymer films

Many literature studies have previously studied the humidity response of CLCs,[16,17,19] so experiments were conducted to explore the difference between the humidity response of CLCs and the humidity response of BP under similar conditions. First, BP and CLCs with the same chiral agent content were prepared, and the reflection peak of the samples of BP and CLCs before IPN treatment was compared (Fig. S5, ESI†). The reflection peak difference between BP and CLCs at the same ratio was approximately 200 nm, while the reflection peak of CLCs was close to the range measured by the instrument. After subjecting to IPN treatment, the reflection peak of the CLC sample was difficult to attain within the visible light spectrum. Therefore, the experimental effect of alkalized acrylic-CLCs directly prepared using the BP formula at low temperature was not the best. By reducing the chirality content (**HTG135200** = 40.0 wt%, **HCM006** = 4.5 wt%, **RM257** = 18.0 wt%), the reflection peak of CLCs before treatment was controlled between 500–600 nm. Then IPN treatment of CLCs was carried out using the method of BP treatment described in sections 4.5–4.7 in this article to obtain alkalized-acrylic-CLCs, which are compared with alkalized acrylic-BP (**HTG135200** = 40.0 wt%, **HCM006** = 6.0 wt%, **RM257** = 18.0 wt%) to investigate the similarities and disparities in their response to humidity.

The humidity response can be observed in both alkalized-acrylic-CLCs and alkalized-acrylic-BP after IPN treatment, as depicted in Fig. 11. Comparing the reflection images of both samples, it was evident that the reflection peaks exhibit a noticeable redshift, with alkalized-acrylic-CLCs displaying a slightly greater variation in amplitude of its reflection peaks compared to alkalized-acrylic-BP. However, the key distinction between the two lies in the fact that alkalized-acrylic-BP exhibited a bimodal distribution owing to its unique lattice structure. In the process of humidity response, one peak of alkalized-acrylic-BP remains stationary, while the other peak exhibits a pronounced red shift. The alkalized-acrylic-CLCs exhibited a single peak, which undergoes a shift upon exposure to humidity. By comparing the polarizing images of both samples in Fig. 11, it is evident that the polarizing images of alkalized-acrylic-BP exhibit blue spots, which remain unaffected by the humidity response. Conversely, the surrounding region undergoes a color transition from green to red due to changes in humidity levels, precisely corresponding to alterations in the reflection peak. As evident from the POM images of alkalized acrylic-CLCs, the color of the CLC polymer's texture undergoes changes in response to humidity; however, no blue spots appear throughout the entire process. By comparing the SEM images of the two surface morphologies the alkalized-acrylic-BP exhibits a blue-phase lattice structure, and the SEM surface of

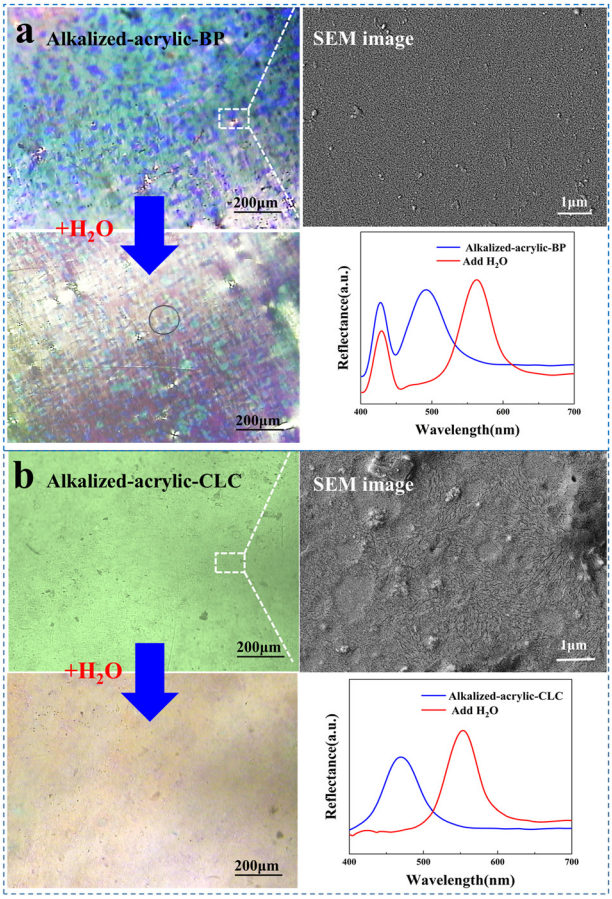

Fig. 11 (a) Comparison of POM and reflection spectra and SEM images of the surface morphology of alkalized-acrylic-BP before and after the humidity response. (b) Comparison of POM, reflection spectrum and SEM image of alkalized acrylic-CLCs before and after the humidity response (alkalized acrylic-BP: **HTG135200** = 40.0 wt%, **HCM006** = 6.0 wt%, and **RM257** = 18.0 wt%; alkalized-acrylic-CLCs: **HTG135200** = 40.0 wt%, **HCM006** = 4.5 wt%, and **RM257** = 18.0 wt%).

the sample demonstrated a significantly denser morphology with a tendency towards point-like features. In the SEM image of alkalized acrylic CLCs, there were many stripes on the surface of the sample, which was similar to the layer thread of the cholesteric phase. The aforementioned evidence demonstrated the discernible structural disparity between the two samples.

3. Conclusions

The present study introduces IPN humidity-responsive blue phase liquid crystal polymer films (alkalized acrylic-BP) for the first time, demonstrating their capability to exhibit both color and deformation responses in accordance with humidity variations. The investigation of film changes during preparation has demonstrated the successful construction of IPN alkalized-acrylic-BP films. The effects of **HTG135200**, **RM257** and **HCM006** on the optical reflectance of the film were analyzed by grouping experiments, and the effects of each factor on $K_{avg}\Delta\lambda$ were calculated. The variation in the **RM257**

content is observed to exhibit a positive correlation with the alteration in optical reflectance. In the actual experiment, to enhance the humidity response performance of the film, the optical reflection can be effectively enhanced by judiciously adjusting the content of the **RM257** crosslinker. A patterned alkalized-acrylic-BP film was also prepared, and the response of ethanol solution with different water contents to the film was investigated. It has been observed that the reflection peak of the film undergoes a continuous red shift within a certain range as the water content increases. A quantitative analysis was conducted to investigate the influence of humidity, film thickness, and **HTG135200** content on the mechanical properties of the film. Furthermore, the polarizing images, the changes of the SEM surface morphology and the changes of the reflection spectra under the influence of humidity of alkalized-acrylic-BP and alkalized-acrylic-CLCs were compared. The present study not only offers novel insights into the underlying mechanism driving the humidity response of IPN blue phase liquid crystal films, but also expands the potential application prospects of BPLC films in electronic devices and sensors. In the future, more potential applications can be explored based on this 3D self-assembled nanomaterial.

4. Experimental section

4.1. Materials

The nematic liquid crystal **HTG135200** and chiral dopant **HCM006** were provided by HCCH. The polymerizable liquid crystal monomers **RM257** and **HCM021** were purchased from Merck. Trimethylol propane trimethacrylate (**TMPTMA**) and photoinitiator **I-651** were obtained from J&K Scientific Ltd. All solvents and chemicals were of reagent quality and can be used without further purification. Clean slides were used to prepare liquid crystal cells.

4.2. Characterization

The phase transition behavior of the mixture was observed using a POM (Eclipse LV120POL, Nikon) equipped with a precision temperature-controlled hot plate (LTS100E, Linkam). The reflection spectrum was obtained using a fiber optic spectrometer (Avantes, AvaSpec-2048). Fourier transform infrared spectra were recorded on a Varian 670 Fourier transform infrared spectrometer with slide-in ATR (Ge), and SEM imaging was performed at the Zeiss Field Emission scanning electron microscope in Germany. Thermogravimetric analysis was performed on the US TA TGA 550.

4.3. LCD substrate functionalization and LCD precursor configuration

With a 70 μm plastic film serving as an interlayer, the two PVA-functionalized glass sheets with surface treatment were stacked and bonded together using an adhesive. The necessary materials, including liquid crystal materials, a monomer, and a photoinitiator, were accurately weighed in a specific proportion. They were then placed into a test tube and mixed with 3 mL of dichloromethane solution before being subjected to ultrasonic treatment for 10 minutes using an ultrasonic cleaner. This process ensured complete dissolution of the mixture to obtain the required liquid crystal precursor. Then put the test tube into the vacuum drying oven (60 °C, 10 h) to let the dichloromethane completely volatilize.

4.4. Preparation of the blue phase liquid crystal polymer film (PS-BP)

The liquid crystal precursor was heated above the temperature of the clear spot, and poured into the cell under the action of capillary force. The cell was placed onto a precision temperature-controlled hot plate. At the beginning, the temperature dropped to a temperature close to that of the blue phase at a speed of 5 °C min^{-1}. Then the temperature was lowered to that of blue phase at 0.05 °C min^{-1}. Heating was carried out for 10 min at a temperature 1.0 °C higher than the phase transition temperature from BP to Ch. After the blue phase texture was stabilized, the sample was irradiated with 365 nm ultraviolet light (a light intensity of 60 mW cm^{-2} and a time of 480 s). Finally, the liquid crystal box was opened and the upper glass sheet was removed to obtain PS-BP.

4.5. Preparation of the blue phase polymer network film (soaked-BP)

After opening the cell, the PS-BP film was immersed in a tetrahydrofuran solution for 30 minutes. After the film was completely swollen and discolored, the small molecule liquid crystal inside has been removed. Then remove the film and add a small amount of anhydrous ethanol to prevent violent contraction and deformation caused by tetrahydrofuran volatilization. Finally, it was dried in a vacuum drying oven (60 °C, 30 min) to obtain soaked-BP.

4.6. Preparation of the interpenetrating acrylic blue phase polymer network film (acrylate-BP)

Firstly, acrylic acid prepolymer solution (acrylic acid : **PEG-DA 600** : **I-651** = 98 : 1 : 1 wt%) was prepared. Soaked-BP was heated on a precision temperature-controlled hot plate at 60 °C, and then dripped acrylic prepolymer solution onto the film with a glue head dropper to completely infiltrate the film and left for 10 min. After the film was completely swollen and deformed, we removed the film from the temperature-controlled hot plate and used a cotton swab to gently wipe off the surface of the film and the excess acrylic prepolymer solution around it. Finally, the sample was irradiated with 365 nm ultraviolet light (light intensity 20 mW m^{-2}, 480 s) to obtain acrylic-BP.

4.7. Preparation of alkalized interpenetrating acrylic blue phase polymer network film (alkalized-acrylic-BP)

Firstly, 0.1 mol L^{-1} KOH solution was prepared, and the acrylic-BP film obtained in the previous step was soaked in 0.1 mol L^{-1} KOH solution for 12 h. After the film was completely removed and curled, subsequently, it was placed in a vacuum drying oven at 60 °C for 30 minutes. The alkalized-acrylic-BP was ultimately obtained.

Author contributions

The article was written through contributions of all authors. All authors have given approval to the final version of the article.

Conflicts of interest

There are no conflicts to declare.

Acknowledgements

This work was supported by the National Natural Science Foundation of China (Grant No. 61370048 and 51673023).

Notes and references

1 F. Liu, S. Zhang, Y. Meng and B. Tang, *Small*, 2020, **16**, 2319–2327.
2 A. J. J. Kragt, N. C. M. Zuurbier, D. J. Broer and A. Schenning, *ACS Appl. Mater. Interfaces*, 2019, **11**, 28172–28179.
3 A. Belmonte, M. Pilz da Cunha, K. Nickmans and A. P. H. J. Schenning, *Adv. Opt. Mater.*, 2020, **8**, 54–62.
4 E. P. A. van Heeswijk, J. J. H. Kloos, N. Grossiord and A. P. H. J. Schenning, *J. Mater. Chem. A*, 2019, **7**, 6113–6119.
5 P. Lv, X. Yang, H. K. Bisoyi, H. Zeng, X. Zhang, Y. Chen, P. Xue, S. Shi, A. Priimagi, L. Wang, W. Feng and Q. Li, *Mater. Horizons*, 2021, **8**, 2475–2484.
6 P. Xue, C. Valenzuela, S. Ma, X. Zhang, J. Ma, Y. Chen, X. Xu and L. Wang, *Adv. Funct. Mater.*, 2023, **4**, 4867–4879.
7 Q. Ya, W.-Q. Chen, X.-Z. Dong, T. Rodgers, S. Nakanishi, S. Shoji, X.-M. Duan and S. Kawata, *Appl. Phys. A: Mater. Sci. Process.*, 2008, **93**, 393–398.
8 Y. J. Liu, Z. Cai, E. S. P. Leong, X. S. Zhao and J. H. Teng, *J. Mater. Chem.*, 2012, **22**, 7609–7614.
9 Y. Li, Y. Chen, D. Yi, Y. Du, W. Luo, X. Hong, X. Li, Y. Geng and D. Luo, *J. Mater. Chem. C*, 2020, **8**, 11153–11159.
10 D. Kou, W. Ma, S. Zhang and B. Tang, *ACS Appl. Polym. Mater.*, 2019, **2**, 2–11.
11 C. Esteves, E. Ramou, A. R. P. Porteira, A. J. M. Barbosa and A. C. A. Roque, *Adv. Opt. Mater.*, 2020, **8**, 117–136.
12 C.-K. Chang, H.-L. Kuo, K.-T. Tang and S.-W. Chiu, *Appl. Phys. Lett.*, 2011, **99**, 55–62.
13 L. Wang and Q. Li, *Adv. Funct. Mater.*, 2016, **26**, 10–28.
14 C.-K. Chang, C. M. W. Bastiaansen, D. J. Broer and H.-L. Kuo, *Adv. Funct. Mater.*, 2012, **22**, 2855–2859.
15 Y. Cao, L. Chong, K.-H. Wu, L.-Q. You, S.-S. Li and L.-J. Chen, *Chin. Opt. Lett.*, 2022, **20**, 602–608.
16 L. Zhang, W. He, Y. Cui, Y. Zhang, Z. Yang, D. Wang, H. Cao and Y. Li, *Liq. Cryst.*, 2022, **49**, 1411–1419.
17 J. E. Stumpel, E. R. Gil, A. B. Spoelstra, C. W. M. Bastiaansen, D. J. Broer and A. P. H. J. Schenning, *Adv. Funct. Mater.*, 2015, **25**, 3314–3320.
18 X. Shi, Z. Deng, P. Zhang, Y. Wang, G. Zhou and L. T. Haan, *Adv. Funct. Mater.*, 2021, **31**, 4641–4651.
19 Y. Liu, B. Xu, S. Sun, J. Wei, L. Wu and Y. Yu, *Adv. Mater.*, 2017, **29**, 1604732.
20 M. Sadati, J. A. Martinez-Gonzalez, A. Cohen, S. Norouzi, O. Guzman and J. J. de Pablo, *ACS Nano*, 2021, **15**, 15972–15981.
21 P. Nayek, H. Jeong, H. R. Park, S.-W. Kang, S. H. Lee, H. S. Park, H. J. Lee and H. S. Kim, *Appl. Phys. Exp.*, 2012, **5**, 1701–1705.
22 J. A. Martinez-Gonzalez, X. Li, M. Sadati, Y. Zhou, R. Zhang, P. F. Nealey and J. J. de Pablo, *Nat. Commun.*, 2017, **8**, 15854–15863.
23 Y. Li, S. Huang, P. Zhou, S. Liu, J. Lu, X. Li and Y. Su, *Adv. Mater. Technol.*, 2016, **1**, 102–130.
24 S. S. Gandhi and L. C. Chien, *Adv. Mater.*, 2017, **29**, 4296–4309.
25 L. Zheng, X.-J. Xu, D.-P. Sun, K.-Y. Du, X. Zhou, Y.-Z. Geng, L. Chen, J.-L. Zhu, D. Chen and W. Han, *ACS Appl. Nano Mater.*, 2022, **5**, 12943–12950.
26 Y. Yang, Y. K. Kim, X. Wang, M. Tsuei and N. L. Abbott, *ACS Appl. Mater. Interfaces*, 2020, **12**, 42099–42108.
27 J. Yang, W. Zhao, Z. Yang, W. He, J. Wang, T. Ikeda and L. Jiang, *J. Mater. Chem. C*, 2019, **7**, 13764–13769.
28 T. Emeršič, K. Bagchi, J. A. Martínez-González, X. Li, J. J. de Pablo and P. F. Nealey, *Adv. Funct. Mater.*, 2022, **32**, 2721–2731.
29 H. Wang, H. Zhou, W. He, Z. Yang, H. Cao, D. Wang and Y. Li, *Materials*, 2022, **16**, 10194–10214.
30 C. Esteves, E. Ramou, A. R. P. Porteira, A. J. M. Barbosa and A. C. A. Roque, *Adv. Opt. Mater.*, 2020, **8**, 2117–2146.
31 W. Hu, J. Sun, Q. Wang, L. Zhang, X. Yuan, F. Chen, K. Li, Z. Miao, D. Yang, H. Yu and H. Yang, *Adv. Funct. Mater.*, 2020, **30**, 4610–4646.
32 Y. Yang, X. Zhang, Y. Chen, X. Yang, J. Ma, J. Wang, L. Wang and W. Feng, *ACS Appl. Mater. Interfaces*, 2021, **13**, 41102–41111.
33 Y. Gao, T. Huang and J. Lu, *Crystals*, 2021, **11**, 602–612.
34 F. Castles, F. V. Day, S. M. Morris, D. H. Ko, D. J. Gardiner, M. M. Qasim, S. Nosheen, P. J. Hands, S. S. Choi, R. H. Friend and H. J. Coles, *Nat. Mater.*, 2012, **11**, 599–603.
35 E. Bukusoglu, X. Wang, J. A. Martinez-Gonzalez, J. J. de Pablo and N. L. Abbott, *Adv. Mater.*, 2015, **27**, 6892–6898.
36 K. Hirotsugu, Y. Masayuki, H. Yoshiaki, Y. Huai and K. Tisato, *Nat. Mater.*, 2002, **1**, 12–23.
37 D. Y. Guo, C. W. Chen, C. C. Li, H. C. Jau, K. H. Lin, T. M. Feng, C. T. Wang, T. J. Bunning, I. C. Khoo and T. H. Lin, *Nat. Mater.*, 2020, **19**, 94–101.
38 A. Lohani, G. Singh, S. S. Bhattacharya and A. Verma, *J. Drug Delivery Sci. Technol.*, 2014, **2014**, 583612.
39 L. Yin, J. Ding, J. Zhang, C. He, C. Tang and C. Yin, *Biomaterials*, 2010, **31**, 3347–3356.
40 F. Gnanaprakasam Thankam, J. Muthu, V. Sankar and R. Kozhiparambil Gopal, *Colloids Surf., B*, 2013, **107**, 137–145.
41 S. J. Kim, S. G. Yoon, S. M. Lee, J. H. Lee and S. I. Kim, *Sens. Actuators, B*, 2003, **96**, 1–5.
42 S. J. Kim, S. J. Park, S. M. Lee, Y. M. Lee, H. C. Kim and S. I. Kim, *J. Appl. Polym. Sci.*, 2003, **89**, 890–894.
43 D. Tang, X. Zhang, L. Liu and L. Qiang, *J. Nanomater.*, 2009, **2009**, 1–6.
44 P. Mehta and B. S. Kaith, *Int. J. Biol. Macromol.*, 2018, **107**, 312–321.

45 Q. Wang, S. Li, Z. Wang, H. Liu and C. Li, *J. Appl. Polym. Sci.*, 2009, **111**, 1417–1425.
46 T. Ube, K. Takado and T. Ikeda, *Mol. Cryst. Liq. Cryst.*, 2014, **594**, 86–91.
47 K. Takado, T. Ube and T. Ikeda, *Mol. Cryst. Liq. Cryst.*, 2014, **601**, 43–48.
48 S. Gwon and S. Park, *J. Ind. Eng. Chem.*, 2021, **99**, 235–245.
49 S. Hussain and S.-Y. Park, *Sens. Actuators, B*, 2020, 316.
50 M. Moirangthem, R. Arts, M. Merkx and A. P. H. J. Schenning, *Adv. Funct. Mater.*, 2016, **26**, 1154–1160.
51 J. Yang, W. Zhao, Z. Yang, W. He, J. Wang, T. Ikeda and L. Jiang, *ACS Appl. Mater. Interfaces*, 2019, **11**, 46124–46131.